JOURNAL OF INFORMATION SCIENCE AND ENGINEERING 33, 429-444 (2017)
DOI:10.1688/JISE.2017.33.2.9

Performance Analysis of Diagonal Permutation Shifting (DPS) Codes for SAC-OCDMA Systems*

HASSAN YOUSIF AHMED[1,+], ZAKARIA MUKHTAR GHARSSELDIEN[2] AND SYED ALWEE ALJUNID[3]
[1]*Electrical Engineering Department*
College of Engineering at Wadi Aldawaser
[2]*Mathematical Department*
College of Art and Science
Prince Sattam Bin Abdulaziz University
Riyadh Region, 11991 Kingdom of Saudi Arabia
[3]*School of Computer and Communication Engineering*
Universiti Malaysia
Perlis, 02600 Malaysia
[+]*E-mail: hassanuofg@gmail.com*

Due to the large bandwidth offered by the optical fiber, its implementation in local area network (LAN) where the traffic is typically bursty could be considered as the strongest candidates for the future high speed optical networks if coding technique is used. This paper presents a new code family named, diagonal permutation shifting (DPS) for spectral amplitude coding-optical code division multiple access (SAC-OCDMA) systems with fixed in-phase cross correlation (CC) and short code length. DPS code derived from well-known prime codes and some matrix operations. The results reveal that the DPS code acts effectively in removing multiple access interface (MAI) and mitigate phase induced intensity noise (PIIN) impact with an adequate signal to interference plus-noise ratio (SINR) and low bit error rate (BER). It has been shown that the DPS code family can suppress intensity noise effectively and improve the system performance significantly.

Keywords: DPS, SAC, OCDMA, MAI, fiber optics

1. INTRODUCTION

Telecommunication system based on optical transmission has taken over the backbone of conventional transmission due to its ability to provide flexible, reliable, affordable and scalable services to user's expectation. The demand for optical communication systems has been rapidly increasing due to the large bandwidth offered by the fiber optic. This demand is fueled by many different factors. Social media and multimedia services comprise moving pictures, static pictures, text, and sound in an interactive environment. At the same time, e-businesses and e-Government are relying increasingly on internet for day to day operations. This is because the internet provides an immediate and accessible set of information, resources and services [1, 2]. Nowadays vast amount of bandwidths are being consuming extensively due to the tremendous growth of the internet which has brought an enormous number of users online dealing with data transfers involve videos,

Received January 1, 2016; revised April 10, 2016; accepted June 1, 2016.
Communicated by Ying-Dar Lin.
* This project was supported by the Deanship of Scientific Research at Prince Sattam bin Abdulaziz University under the research project # 2014/1/877.
+ Corresponding author.

database queries, updates and images [1-7]. These demands have driven the necessity to replace conventional low-capacity copper access links to higher-capacity connections. To realize the demands for bandwidth and new services, a new technology must be deployed and fiber optic is one such key technology [8]. Optical fiber offers many advantages over conventional media (*e.g.* coaxial cable and twisted pair). It offers unlimited bandwidth and is considered as the ultimate solution to deliver broadband access to the last mile. It also offers a much lower attenuation factor where optical signals can be transmitted over very long distances without signal regeneration or amplification [8-11]. In addition, many channels can be multiplexed to share the same fiber optic medium and thus reducing the number of links required and the cost to end users [12]. Therefore, fiber optic systems could be the answer to many urgent needs of the telecommunication systems, as they could provide the necessary bandwidth for the transmission of broadband data to the end users. Code ddivision mmultiple access (CDMA) is the most recent multiple accessing technique in the optical domain [10, 11]. An optical code division multiple access (OCDMA) is a multi access scheme that is based on assigning a distinctive code sequence to each user [1]. However, for highly populated OCDMA network multiple access interference (MAI) is the main reason for performance degradation. Many OCDMA techniques used different approaches to reduce the impact of the MAI. Among these approaches, spectral amplitude-coding (SAC) system draws more attention since the MAI can be completely eliminated by spectral coding through balance detection technique [2-11].

Thanaa Hussein Abd *et al.* [7] proposed dynamic cyclic shift (DCS) code which shows better performance when compared with the reported SAC–OCDMA systems. Although, the code length is short, the requirement of number of users equals to the code length limits the choice of code selection. In order to achieve the cyclic shift property with a minimum cross-correlation ($\lambda_c <= 1$), they always consider the dynamic part $D > 7$; otherwise, the cross-correlation value would have been larger than one.

H. A. Fadhil *et al.* [9] proposed random diagonal (RD) code for OCDMA systems. They used code segment and data segment in code structure which makes the code constructions are easy with shorter code length. However, when the number of users increases the cross correlation increases, eventually degrades the system performances. In addition the notion that the code weight can be any number >3 limits the free cardinality of code selection. On the other hand, as long as the value of the in-phase cross-correlation between code sequences is large, phase-induced intensity noise (PIIN) arising from the square law photo detection of broadband source is another problem leads to system performance deterioration [2-4]. In particular an MAI impact could be eliminated if code with fixed cross correlation is used by using subtraction technique since the code sequence of each interfering user produces the same values in both photodiodes (PDs) of the balanced detector [2, 3]. In this paper an efficient method is used to construct DPS code family with fixed in-phase cross correlation. DPS code derived from well-known prime codes and some matrix operations and is characterized by (L, N, P, λ_c) with code length L, the number of users N, code weight P (number of marks) and cross correlation λ_c. We can highlight the added values and contribution to the spectral-amplitude coding field of optical code-division multiple access (OCDMA) system in this paper as follows: (1) We have proposed a new diagonal permutation shift (DPS) code with ideal in-phase CC; (2) SINR and BER derivations; (3) Any prime number can be used for code weight;

(4) Numerical results compared to RD and DCS codes show significant improvement when DPS code is used.

The remaining parts of this paper are structured as follows. A mathematical model of the DPS code construction and its features are described in Section 2. Section 3 shows the DPS's performance analysis. Calculated results and simulation results are elaborated in Section 4. Study findings are drawn in Section 5.

2. CODE CONSTRUCTION AND CODE PROPERTIES

The aim of this proposed Diagonal-Permutation-Shift (DPS)'s algorithm is to generate code sequences by using some simple algebraic ways and matrix operations to mitigate the influences of both MAI and PIIN for further improvement. This algorithm is derived from the well-known prime code sequences which come from the Galois Field (GF) [2, 3]. DPS code sequences can be generated from GF (P) = {0, 1, 2, …, P – 1} for $P > 2$ where P is a prime number. The following steps are used to construct DPS code family.

Step 1 (Diagonal process): Construct primary diagonal $\alpha_{i,i}$ sequences of integer numbers as shown in Table 1 using Eq. (1).

$$\alpha_{i,j} = (i \cdot j) \bmod P \tag{1}$$

where i and j represent the position of each element over Galois fields and mod represents the modulo operation. Based on Eq. (1), a generator sequence D_P is constructed as follows.

$$D_P = \{\alpha_{0,0}\ \alpha_{1,1}\ \alpha_{2,2}\ \ldots\ \alpha_{P\text{-}1,P\text{-}1}\} \tag{2}$$

For any P the following elements are fixed

$$\left.\begin{aligned} \alpha_{0,0} &= 0, \qquad \alpha_{1,1} = 1 \\ \alpha_{P-1,P-1} &= (P-1)\cdot(P-1)\bmod(P) \\ &= (P^2 - 2P + 1)\bmod(P) = 1 \end{aligned}\right\} \tag{3}$$

Table 1. Tabular representation of integer numbers over GF(*P*).

$i\backslash j$	0	1	2	…	P–1
0	0	0	0	…	0
1	0	1	2	…	P–1
2	0	2	4		P–2
⋮	⋮	⋮	⋮	⋱	⋮
P–1	0	P–1	P–2	…	1

For P = 3, 5 and 7, the following sequences are generated based on Eq. (2).

$$\left.\begin{aligned} D_3 &= \{0\ \ 1\ \ 1\} \\ D_5 &= \{0\ \ 1\ \ 4\ \ 4\ \ 1\} \\ D_7 &= \{0\ \ 1\ \ 4\ \ 2\ \ 2\ \ 4\ \ 1\} \end{aligned}\right\} \tag{4}$$

Step 2 (Permutation process):

Construct the basic matrix B_P^0 by taking D_P as a first row, then make a permutation of D_P one time in the next rows to get a $P\times P$ zero-diagonal symmetric matrix without repeating any row as follows.

$$B_P^0 = \begin{pmatrix} \alpha_{0,0} & \alpha_{1,1} & \alpha_{2,2} & \cdots & \alpha_{P-1,P-1} \\ \alpha_{P-1,P-1} & \alpha_{0,0} & \alpha_{1,1} & \cdots & \alpha_{P-2,P-2} \\ \alpha_{P-2,P-2} & \alpha_{P-1,P-1} & \alpha_{0,0} & \cdots & \alpha_{P-3,P-3} \\ \vdots & \vdots & \vdots & \ddots & \vdots \\ \alpha_{1,1} & \alpha_{2,2} & \alpha_{3,3} & \cdots & \alpha_{0,0} \end{pmatrix} \tag{5}$$

For P = 3, 5 and 7 the following matrices are obtained based on Eq. (5).

$$B_3^0 = \begin{pmatrix} 0 & 1 & 1 \\ 1 & 0 & 1 \\ 1 & 1 & 0 \end{pmatrix}, \tag{6}$$

$$B_5^0 = \begin{pmatrix} 0 & 1 & 4 & 4 & 1 \\ 1 & 0 & 1 & 4 & 4 \\ 4 & 1 & 0 & 1 & 4 \\ 4 & 4 & 1 & 0 & 1 \\ 1 & 4 & 4 & 1 & 0 \end{pmatrix}, \tag{7}$$

$$B_7^0 = \begin{pmatrix} 0 & 1 & 4 & 2 & 2 & 4 & 1 \\ 1 & 0 & 1 & 4 & 2 & 2 & 4 \\ 4 & 1 & 0 & 1 & 4 & 2 & 2 \\ 2 & 4 & 1 & 0 & 1 & 4 & 2 \\ 2 & 2 & 4 & 1 & 0 & 1 & 4 \\ 4 & 2 & 2 & 4 & 1 & 0 & 1 \\ 1 & 4 & 2 & 2 & 4 & 1 & 0 \end{pmatrix} \tag{8}$$

Step 3 (Shifting process): Construct (P–1) shifted matrices B_P^k by adding k to each element of the matrix B_P^0, where k = 1, 2, …, P–1. In doing so, the following metrics are obtained in Eqs. (9) and (10) for P = 3.

$$B_3^1 = \begin{pmatrix} 1 & 2 & 2 \\ 2 & 1 & 2 \\ 2 & 2 & 1 \end{pmatrix} \tag{9}$$

$$B_3^2 = \begin{pmatrix} 2 & 0 & 0 \\ 0 & 2 & 0 \\ 0 & 0 & 2 \end{pmatrix} \tag{10}$$

Step 4 (Joining process): In joining process, the matrix A is obtained by joining B_P^k in each sequence then an extra column of matrix m_p is added to each corresponding B_P^k.

$$A = \left(\begin{array}{c|c} \left[B_P^0 \right] & \left[m_P \right] \\ \left[B_P^1 \right] & \left[m_P \right] \\ \vdots & \vdots \\ \left[B_P^{P-1} \right] & \left[m_P \right] \end{array}\right), \tag{11}$$

where m_P is a $P\times 1$ matrix contains the elements {0, 1, 2, …, P – 1} in arbitrary order. The size of matrix A is $P^2\times(P+1)$ and its elements A_{ij} where i = 0, 1, 2, …, P^2–1, and j =

0, 1, 2, …, P.

The above four steps can be summarized in Eq. (12). This equation is valid for any prime number $P > 2$ to generate a code with a unity cross correlation in the form of a matrix.

$$\left.\begin{aligned} A_{i,j} &= \left(S_w.\left[\left(j - i_P\right)^{P+1} + \frac{i - i_P}{P} \right] + i_P \frac{j - j_P}{P} \right) \bmod P \\ i_P &= i \bmod P, \qquad j_P = j \bmod P, \\ k_P &= k \bmod P, \qquad S_w = \lim_{k \to j} \frac{k_P}{k} \end{aligned}\right\} \tag{12}$$

The properties of DPS code are mentioned as follows.

An ideal CC between any sequences; the number of users $N = P^2$; the weight is a prime number greater than 2; the code length equals P^2+P; each code sequence has (P+1) "1s" and (P^2–1) "0s".

In the case of $P = 3$, Eq. (12) is applied to calculate the values of $A_{i,j}$ which are listed in Tables 2-4. These calculated values are used to build the DPS code patterns shown in Table 5.

Table 2. $i = 2$.

j	0	1	2	3
i_p	0	0	0	0
j_p	0	1	2	0
S_w	1	1	1	0
$A_{0,j}$	0	1	1	0

Table 3. $i = 2$.

j	0	1	2	3
i_p	1	1	1	1
j_p	0	1	2	0
S_w	1	1	1	0
$A_{0,j}$	1	0	1	1

Table 4. $i = 2$.

j	0	1	2	3
i_p	2	2	2	2
j_p	0	1	2	0
S_w	1	1	1	0
$A_{0,j}$	1	1	0	2

Table 5. DPS code sequences for $P = 3$.

i	$A_{i,j}$ j:0123	DPS code			
0	0110	100	010	010	100
1	1011	010	100	010	010
2	1102	010	010	100	001
3	1220	010	001	001	100
4	2121	001	010	001	010
5	2212	001	001	010	001
6	2000	001	100	100	100
7	0201	100	001	100	010
8	0022	100	100	001	001

3. PERFORMANCE ANALYSIS OF THE DPS CODE SYSTEM

Fig. 1 shows the transmitter/receiver structure based on the DPS code sequence for $P = 3$. On the transmitter side (Fig. 1 (a)), the information of user#1, coded as 100010010100, as listed in Table 5 is modulated using the ON-OFF Keying (OOK).

The signal is then directed to an FBG set, where each chip of the desired user is being attributed with a specific wavelength (λ_1 λ_5 λ_8 λ_{10}). The center wavelengths of the

FBGs depend on the positions of the mark chips in the code sequences. In Fig. 1 (b) the incoming signal is decoded by the decoder which has an identical spectral response to the intended encoder for the data to be recovered (Decoder) [3]. The detected output (the intended signal spectrum and overlapping spectra from other interferers) from the decoder is P+1 power units for the desired user accompanied by λ power units for interferers.

The complementary decoder (Comp-Decoder) branch detects the complementary spectrum of the intended user (from Table 5, λ_2 λ_3 λ_4 λ_6 λ_7 λ_9 λ_{11} λ_{12}); where the received signal is passed through FBG sets and the result circulated to a balanced photo-detectors [3]. From the FBGs, different center wavelengths are placed along a piece of fiber and the wavelength elements of spectral codes are spread out in time. So, second fibers with FBGs in reverse positions are needed in each encoder and decoder in order to compensate the time spreading. In order to differentiate between the wanted and unwanted signals, a subtractor is used to subtract overlapping signals from the wanted signal to reproduce the desired signal. Finally, after photo detections, low pass filter (LPF) and thresholding, the original data is recovered.

If $C_f(i)$ denotes the ith element of the fth DPS code sequence, the code properties based on XOR subtraction technique can be written as [4]:

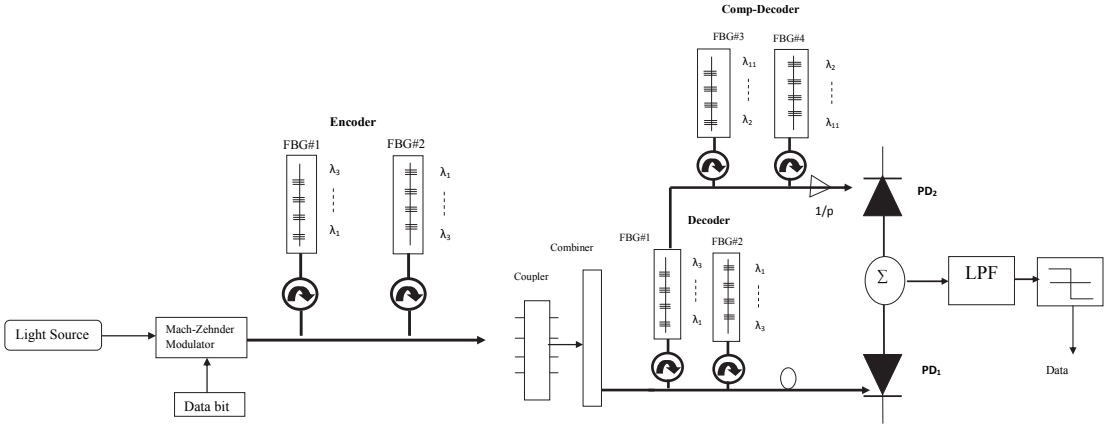

(a) (b)

Fig. 1. Implementation of the Complementary detection technique using DPS code; (a) Transmitter; (b) Receiver; PD_1 and PD_2: photodiodes. LPF: low pass filter.

$$\sum_{i=1}^{L} C_f(i) \cdot C_g(i) = \begin{cases} P+1, & f = g \\ 1, & f \neq g \end{cases} \tag{13}$$

and

$$\sum_{i=1}^{L} C_f(i) \cdot (C_f(i) \oplus C_g(i)) = \begin{cases} 0, & f = g \\ P, & f \neq g \end{cases} \tag{14}$$

where $\oplus$ represents XOR operation. The condition of $f = g$ meaning the desired user while the condition $f \neq g$ meaning the interference's user when $CC = 1$. Therefore, the XOR operation of $(C_f(i) \oplus C_g(i))$ is valid for $f \neq g$ only. However, the cross correlation of

$C_f(i) \cdot (C_f(i) \oplus C_g(i))$ is valid for $f \neq g$ only in Eq. (14) while from Eq. (13), the cross correlation of $C_f(i) \cdot C_g(i)$ is P+1 when $f = g$. Consequently, the MAI can be eliminated as the cross correlation $\sum_{i=1}^{L} C_f(i) \cdot (C_f(i) \oplus C_g(i))$ can be subtracted from $\sum_{i=1}^{L} C_f(i) \cdot C_g(i)$ when $f \neq g$. Therefore, the decoder that computes Eq. (15) rejects the MAI coming from interfering users and obtains the desired information bits.

Thus

$$\sum_{i=1}^{L} C_f(i) \cdot C_g(i) - \frac{\sum_{i=1}^{L} C_f(i) \cdot (C_f(i) \oplus C_g(i))}{P} = \begin{cases} P+1, & f = g \\ 0, & f \neq g \end{cases} \tag{15}$$

Hence, the weight is zero when $f \neq g$, meaning MAI can be fully removed by using XOR subtraction detection technique.

To clarify Eq. (15), the logical representation of MAI cancellation for DPS code is presented in Table 6 based on the information of user#1, coded as **100010010100** and the information user#2, coded as **010100010010** shown in Table 6.

Table 6. Logical representation of MAI cancellation for DPS code.

	Code sequences
Desired User (DU)	{100010010100 }
Interfering User (IU)	{010100010010}
$DU \bullet IU$	{0000000**1**0000}
$\sum DU \bullet IU$	1
Complementary of DU (CDU)	{ 011101101011}
IU	{ 010100010010}
$\sum CDU \bullet IU$	111
$\frac{\sum CDU \bullet IU}{p}$	$\frac{1\ 1\ 1}{1\ 1\ 1} = 1$
$\sum DU \bullet IU - \frac{\sum CDU \bullet IU}{p}$	1-1 = 0

When a broad-band pulse is input into the group of FBGs, the incoherent light fields are mixed and incident upon a photo-detector, the phase noise of the fields causes an intensity noise term in the photo-detector output [4-6]. The coherence time of a thermal source (τc) is given by [4]:

$$\tau_c = \frac{\int_0^{\infty} G^2(v)\,dv}{\left[\int_0^{\infty} G(v)\,dv\right]^2} \tag{16}$$

where $G(v)$ is the single sideband power spectral density (PSD) of the source. The variance of photocurrent due to the detection of an ideally unpolarized thermal light,

which is generated by spontaneous emission, can be written as:

$$\langle i^2 \rangle \quad = \langle I_{shot}^2 \rangle \; + \left\langle I_{PIIN}^2 \right\rangle + \langle I_{thermal}^2 \rangle \tag{17}$$

where I_{shot}^2 denotes shot noise, I_{PIIN}^2 represents phase induced intensity noise and $I_{thermal}^2$ is the thermal noise. Thus, Eq. (18) can also be written as:

$$\langle i^2 \rangle = 2eIB + I^2 B\tau_c + 4K_B T_n B R_L \tag{18}$$

where, e = electron charge; I = average photocurrent; τ_c = coherence time of source; B = noise-equivalent electrical bandwidth of the receiver; K_B = Boltzmann's constant; T_n = absolute receiver noise temperature; R_L = receiver load resistor.

In Eq. (18), the first term results from the shot noise, the second term denotes the effect of phase intensity induced noise (PIIN) [4-6], and the third term represents the effect of thermal noise. The total effect of PIIN and shot noise obeys negative binomial distribution [4]. To analyze the system with transmitter and receiver, we used the same assumptions that were used in [4, 5]. Without these assumptions, it is difficult to analyze the system. We assume the following: (1) Each light source is ideally unpolarized and its spectrum is flat over the bandwidth $v_o \pm \frac{\Delta v}{2}$, where v_o is the central optical frequency and Δv is the optical source bandwidth in Hertz; (2) each power spectral component has identical spectral width; each user has equal power at the receiver; each bit stream from each user is synchronized.

The above assumptions are important for mathematical simplicity. In Eq. (18), the total effect of PIIN and shot noise obeys negative binomial distribution, and thermal noise has a Gaussian distribution. Therefore, Gaussian approximation is used for all of them to easily analyze the system performance [4].The power spectral density (PSD) of the received optical signals can be written as [5, 6]:

$$r(v) = \frac{P_{sr}}{\Delta v} \sum_{n=1}^{N} d_n \sum_{i=1}^{L} c_n(i)\, rec\,(i) \tag{19}$$

where P_{sr} is the effective power of a broad-band source at the receiver, N is the number of users, d_n is the data bit of the nth user that is "1" or "0", and L is the DPS code length. The $rec(i)$ function in Eq. (19) is given by

$$rec\,(i) = u\left[v - v_o - \frac{\Delta v}{2L}(-L + 2i - 2) \right] - u\left[v - v_o - \frac{\Delta v}{2L}(-L + 2i) \right] \tag{20}$$

where $u[v]$ is the unit step function expressed as:

$$u[v] = \begin{cases} 1, & v \geq 0 \\ 0, & v < 0 \end{cases} \tag{21}$$

The total power incident at the input of PD_1 and PD_2 of Fig. 1 of the gth receiver during one bit period is given by

$$\begin{aligned}\int_0^\infty G_1(v)dv &= \int_0^\infty \frac{P_{sr}}{\Delta V}\sum_{f=1}^{N} d_f \sum_{i=1}^{L} c_f(i)c_g(i)\begin{pmatrix} u\left[v-v_o-\frac{\Delta v}{2L}(-L+2i-2)\right] \\ -u\left[v-v_o-\frac{\Delta v}{2L}(-L+2i)\right]\end{pmatrix}dv \\ &= \frac{P_{sr}}{\Delta V}\frac{\Delta v}{L}\sum_{f=1}^{N} d_f \sum_{i=1}^{L} c_f(i)\,c_g(i) \\ &= \frac{P_{sr}(P+1)}{L}d_g + \frac{P_{sr}}{L}\sum_{f=1,f\neq g}^{N} d_f\end{aligned} \tag{22}$$

$$\begin{aligned}\int_0^\infty G_2(v)dv &= \int_0^\infty \frac{P_{sr}}{\Delta V}\sum_{f=1}^{N} d_f \sum_{i=1}^{L} \frac{c_f(i)\left(c_f(i)\oplus c_g(i)\right)}{P}\begin{pmatrix} u\left[v-v_o-\frac{\Delta v}{2L}(-L+2i-2)\right] \\ -u\left[v-v_o-\frac{\Delta v}{2L}(-L+2i)\right]\end{pmatrix}dv \\ &= \frac{P_{sr}}{\Delta V}\frac{\Delta v}{L}\sum_{f=1}^{N} d_f \sum_{i=1}^{L} \frac{c_f(i)\left(c_f(i)\oplus c_g(i)\right)}{P} \\ &= \frac{P_{sr}}{L}\sum_{f=1,f\neq g}^{N} d_f\end{aligned} \tag{23}$$

The signal from desired user is given by the difference of photodiode current I, expressed as

$$I = I_1 - I_2 \tag{24}$$

where I_1, I_2 are the currents at PD_1 and PD_2, respectively.

$$\begin{aligned}I &= \Re\int_0^\infty G_1(v)dv - \Re\int_0^\infty G_2(v)dv \\ &= \Re\left(\frac{P_{sr}(P+1)}{L}d_g + \frac{P_{sr}}{L}\sum_{f=1,f\neq g}^{N} d_f - \frac{P_{sr}}{L}\sum_{f=1,f\neq g}^{N} d_f\right) \\ &= \Re\left(\frac{P_{sr}(P+1)}{L}d_g\right)\end{aligned} \tag{25}$$

where $\Re$ is the responsivity of the photodetectors given by

$$\Re = \frac{\eta e}{hV_c}. \tag{26}$$

Here, η is the quantum efficiency, e is the electron charge, h is the Planck's constant, and V_c is the central frequency of the original broad-band optical pulse. The noise power of shot noise can be written as:

$$\begin{aligned}\left\langle I_{shot}^2\right\rangle &= 2eB\Re\left[\int_0^\infty G_1(v)dv + \int_0^\infty G_2(v)dv\right] \\ &= 2eB\Re\left(+\frac{P_{sr}}{L}\sum_{f=1,f\neq g}^{N} d_f + \frac{P_{sr}}{L}\sum_{f=1,f\neq g}^{N} d_f\right)\end{aligned}$$

$$= 2eB\Re\frac{P_{sr}}{L}\left((P+1)d_g + 2\sum_{f=1, f\neq g}^{N} d_f\right)$$

$$= 2eB\Re\frac{P_{sr}}{L}\left((P+1)+2(N-1)\right)$$

$$\left\langle I_{shot}^2\right\rangle = 2eB\Re\frac{P_{sr}}{P^2+P}\left[2(N-1)+(P+1)\right] \tag{27}$$

Using the same method described in [2, 3] and approximating the summation from Eq. (18), when all the users are transmitting bit '1' using the average value as $\sum_{f=1}^{N} C_f \approx \frac{N(P+1)}{L}$ and from the properties of DPS code the noise power of PIIN can be written as:

$$\langle I_{PIIN}^2\rangle = BI_1^2\tau_{c1} + BI_2^2\tau_{c2}$$

$$= B\Re^2\left[\int_0^{\infty} G_1^2(v)dv + \int_0^{\infty} G_2^2(v)dv\right]$$

$$= B\Re^2\frac{P_{sr}^2}{\Delta vL}\sum_{i=1}^{L}\left\{C_g(i)\left[\sum_{f=1}^{N} d_f C_f(i)\right].\left[\sum_{m=1}^{N} d_m C_m(i)\right]\right\}$$

$$+\frac{B\Re^2}{P^2}\frac{P_{sr}^2}{\Delta vL}\sum_{i=1}^{L}\left\{\left(C_f(i)\oplus C_g(i)\right)\left[\sum_{f=1}^{N} d_f C_f(i)\right]\left[\sum_{m=1}^{N} d_m C_m(i)\right]\right\}$$

$$\cong B\Re^2\frac{P_{sr}^2}{\Delta vL}\sum_{i=1}^{L}\left\{C_g(i)\frac{N(P+1)}{L}\left(\sum_{f=1}^{N} C_f(i)\right)\right\}$$

$$+\frac{B\Re^2}{P^2}\frac{P_{sr}^2}{\Delta vL}\sum_{i=1}^{L}\left\{\left(C_f(i)\oplus C_g(i)\right)\frac{N(P+1)}{L}\left(\sum_{f=1}^{N} C_f(i)\right)\right\}$$

$$\cong B\Re^2\frac{P_{sr}^2}{\Delta vL}\frac{N(P+1)}{L}\sum_{f=1}^{N}\left(\sum_{i=1}^{L} C_f(i)\cdot C_g(i)\right)$$

$$+\frac{B\Re^2}{P^2}\frac{P_{sr}^2}{\Delta vL}\frac{N(P+1)}{L}\sum_{f=1}^{N}\left(\sum_{i=1}^{L} C_f(i)\cdot\left(C_f(i)\oplus C_g(i)\right)\right)$$

$$\langle I_{PIIN}^2\rangle \cong B\Re^2\frac{P_{sr}^2}{\Delta vL}\frac{N(P+1)}{L}\left(P+1+N-1\right)+\frac{B\Re^2}{P^2}\frac{P_{sr}^2}{\Delta vL}\frac{N(P+1)}{L}\left((N-1)\cdot P\right)$$

$$= \frac{B\Re^2 P_{sr}^2 N(P+1)}{\Delta vL^2}\left(P+N+\frac{(N-1)}{P}\right) \tag{28}$$

Noting that the probability of sending bit '1' at any time for each user is ½, then Eqs. (27) and (28) become respectively [4]:

$$\left\langle I_{shot}^2\right\rangle = eB\Re\frac{P_{sr}}{L}\left[2(N-1)+(P+1)\right] \tag{29}$$

$$\langle I_{PIIN}^2\rangle = \frac{B\Re^2 P_{sr}^2 N(P+1)}{2\Delta vL^2}\left(P+N+\frac{(N-1)}{P}\right) \tag{30}$$

The thermal noise is given as [2, 3]:

$$\left\langle I_{thermal}^2 \right\rangle = \frac{4K_b T_n B}{R_L} \tag{31}$$

The SINR of the DPS system can be written as

$$SNR = \frac{I^2}{\left\langle i^2 \right\rangle} = \frac{\left(I_2 - I_1\right)^2}{\left\langle I_{shot}^2 \right\rangle + \left\langle I_{PIIN}^2 \right\rangle + \left\langle I_{thermal}^2 \right\rangle} \tag{32}$$

Thus Eq. (32) based on Eqs. (25), (29)-(31) can be written as:

$$SINR = \frac{\Re^2 P_{sr}^2 (P+1)^2 / L^2}{\left(P_{sr.}\, e\, B\, \Re / L\right)\left[2N + P - 1\right] + \left(B\Re^2 P_{sr.}^2 N(P+1) / (2\Delta\nu L^2)\right)\left(P + N + \dfrac{(N-1)}{P}\right) + 4K_b T_n B / R_L} \tag{33}$$

The Gaussian approximation is used to calculate the bit error rate (BER) based on SINR as in Eq. (33) [5, 6, 11].

$$P_e = \frac{1}{2} erfc\left(\sqrt{\frac{SNR}{8}}\right) \tag{34}$$

4. RESULTS AND DISCUSSION

A sufficient amount of SINR is important in any communication system because it reflects the reliability of the system in general. The SINR is the average of dividing the signal power by the total signal impairment power. BER and SINR are interconnected: a good BER result from a better SINR. A comprehensive discussion will be carried out in the following paragraphs to elaborate the numerical results by using SINR and BER equations while the simulation results will be obtained by using VPI simulator software. The parameters used in our analysis are electrical bandwidth B = 311 MHz; operation wavelength λ_0 = 1550 nm; absolute receiver noise temperature T_n = 300 K; line-width of the thermal source V_c = 3.75 THz; data bit rate R_b = 622 Mb/s; receiver load resistor 1030 Ω; PD quantum efficiency;

In Fig. 2 the SINR is plotted versus the number of users for the DPS (P = 5), DCS (W = 7) and RD (W = 7) codes. The effects of intensity noise, shot noise and thermal noise have been considered when the effective power for each user is equal to -10dBm with an electrical bandwidth of 311 MHz. It is shown that the DPS code gives much higher SINR than DCS and RD with the same code weight. This is because of DCS and RD codes used with a fixed in-phase cross-correlation exactly equal to one and two respectively for suppressing the effect of PIIN. In addition, DCS code always considers the dynamic part $D > 7$; otherwise, the cross-correlation value would have been larger than one while the cross correlation is two for RD code as the number of simultaneous users increases. However, since the in-phase cross-correlation of these codes is always greater than one, the PIIN induced in the system employing these codes is still significant, thus

limiting the system performance. It is reported that higher SINR can be achieved by the DPS code for $P = 7$ than that of $W = 7$. Higher SINR can be obtained with the big values of W thus accommodated a high number of active users.

In Fig. 3, Typically, the BER (*i.e.*, the fraction of incorrectly transmitted bits) is strongly dependent on the transmitted power, and the latter must be sufficient enough to keep the BER below a certain acceptable level (*e.g.* 10^{-12} for digital communication systems). In Fig. 2, the BER is plotted against the number of active users when P_{sr} = −10dBm at 622Mb/s by considering SINR and SIR for DPS, DCS and RD codes. From the figure, it is observed that the BER of DPS code is lower compared to the DCS and RD codes for SINR and SIR.

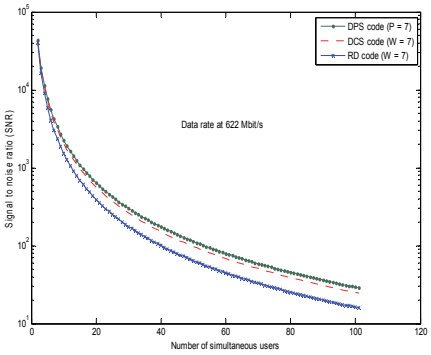

Fig. 2. SINR versus number of active users when P_{sr} = −10dBm at 622Mb/s.

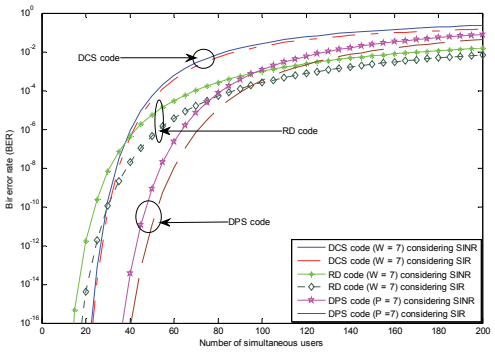

Fig. 3. BER versus number of active users when P_{sr} = −10dBm at 622Mb/s.

An acceptable BER of error free transmission of 10^{-12} was achieved for active users by the DPS code with ≈ 40 (SINR) and ≈ 38 (SIR), DCS code with ≈ 22 (SINR) and ≈ 21 (SIR), and RD code with ≈ 18 (SINR) and ≈ 15 (SIR). This is evident from the fact that DPS code has an in-phase cross correlation property that would eliminate the MAI effects by reducing the power of interference from other users. As a conclusion, the MAI noise is the main reason that impairs the signal than thermal noise and shot noise. Thus SINR has more impact in system performance than SIR because SIR is apart from SINR and this appears in slightly different between SINR and SIR curves for all codes.

Fig. 4 shows the BER versus the effective power P_{sr} when the number of active users is 20 at data rate of 622Mbits/s taking into account the effects of the intensity noise, thermal noise and shot noise for DPS, DCS and RD codes. DPS, DCS and RD codes are adopted with the parameter $P = 7$, while for DCS and RD codes the parameters are $W = 7$ respectively.

The figure shows that the effective power up of the acceptable BER at error free transmission for the DPS code is lower than that for the DCS and RD codes when the number of active users is the same. As a mean of comparison, the DPS reached a 10^{-18} BER at received power −10 dBm, while DCS and RD achieved 10^{-13} and 10^{-11} at the same received power. This is because the interference from other users is fixed to one for the DPS code, while for DCS and RD codes are two respectively as the number of simultaneous users increases.

A block diagram for two users is demonstrated in Fig. 5. Virtual Photonic Instrument (VPI^{TM}) version 7.1 simulation software is used to carry out the tests [11]. In this figure, each laser CW represents a one "1" with a 0.8 nm (100GHz) as the spectral width of each chip. Three laser CWs were used for user#1 and three laser CWs used for user#2. The broadband source is set to −10 dBm. The tests were conducted for various distances with the ITU-T G.652 Non Dispersion Shifted Fiber (NDSF) single mode fiber (SMF) standard. At 1550 nm wavelength, the attenuation coefficient was 0.25 dB/km, and the chromatic dispersion coefficient was 18ps/nm-km and the polarization mode dispersion (PMD) coefficient was 5 ps/km. To mimic the real environment as close as possible, the effects of four-wave mixing (FWM), the self phase modulation (SPM), and the group delay were activated according to the typical industry values. A pseudo random bit sequence (PRBS) generator was used at transmitter side as the input data of each user followed by a coder jitter to generate an NRZ sample finished with a rise time to tune the rise time of the pulse. A Mach-Zehnder modulator was used to modulate the laser output. Fiber Bragg gating (FBG) groups were used to decode the coded sequence words. An ideal clock recovery was used to synchronize the received optical signal with the transmitted signal. An extra clock recovery was used before the photo detectors to synchronize incoming optical signal from desired user and its complementary. A photo detector (PD) is used to decode the coded signal followed by a 0.7 GHz LPF and error detection respectively. The incoming signal was divided into two portions; one to the decoder that matches the structure of the encoder filter; the second portion is decoded by the complementary filter structure of the encoder. A subtractor is used to subtract the output of lower photodiode from the output of upper photodiode then a 0.7 GHz LPF and finally electrical oscilloscope to plot an eye diagram pattern [3, 11].

The eye diagram of DPS at 2.5 Gbit/s for a distance of 30 km is shown in Fig. 6. It clearly demonstrates that even at high data rate, the system employing DPS code is able to detect desired signals with minor distortion due to the fiber nonlinearities parameters. The computed BER versus channel spacing width is shown in Fig. 7 for a 30km fiber length. The pulse duration is fixed to T_c = 1/(data rate × code length) [9]. As the channel spacing width goes from very narrow to wide, the BER decreases, best performance occurs at a spacing bandwidth between 0.8 (100 GHz) and 1.2 nm.

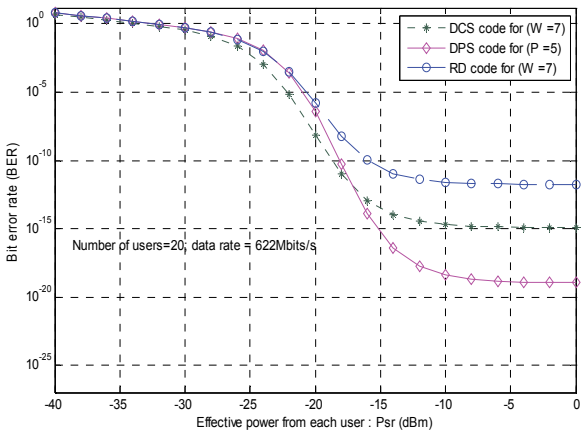

Fig. 4. BER versus effective source power P_{sr} when the number of active users is 20, taking into account the intensity noise, shot noise, and thermal noise at the data rate 622Mb/s.

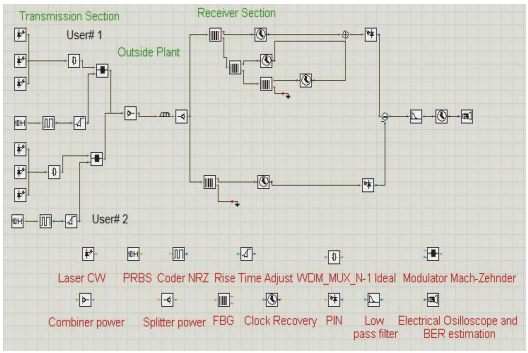

Fig. 5. Simulation setup for the OCDMA system with Complementary technique [9].

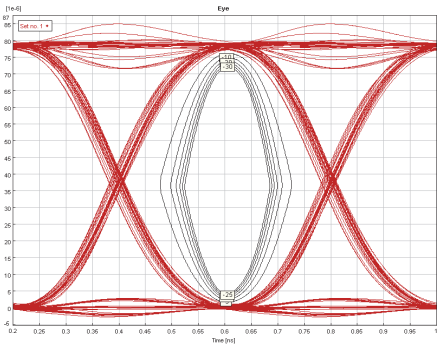

Fig. 6. Eye diagram of DPS code with complementary detection scheme at 2.5 Gbit/s after 30 km.

The reason for the BER increasing after the minimum is that the SINR improvement due to the use of wider optical bandwidth is counteracted by an increased crosstalk/ overlapping between adjacent frequency bins that yield MAI. Note that, decreasing channel spacing the effects of four-wave mixing on optical transmission and in single mode fiber are appeared, this is noticeable as degradation of optical SINR and the system BER performance.

Fig. 8 shows the bit error rate versus the number of active users for the proposed codes with weight 3 and data rate 622 Mbits/s for both simulation and analytical results. In this case the interference noise, shot noise and thermal noise have been considered. These results are obtained for a system with the parameters listed in Table 7 and VPI simulator. One can observe the good matching between the simulation and analytical results.

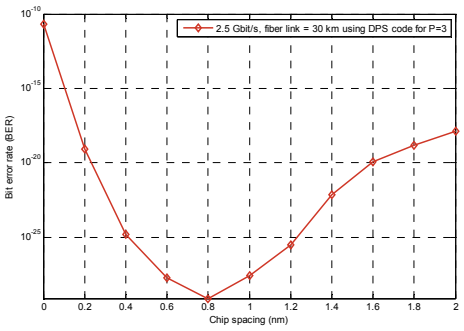

Fig. 7. Variation of BER as a function of channel spacing width for DPS code when (P = 3, N = 9, and L = 12, data rate 2.5 Gbits/s) for a 30km fiber length.

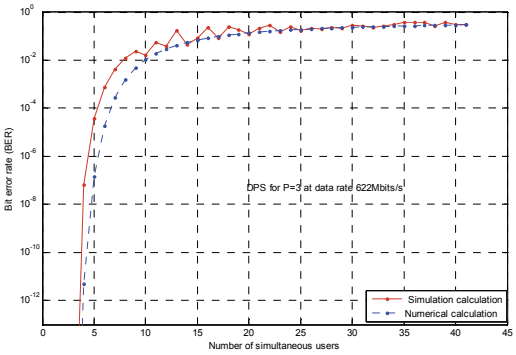

Fig. 8. BER plotted against the number of active users

5. CONCLUSION

In this paper, we have proposed a new code family with cross correlation value of 1, which is considered as an ideal value [5, 6]. The advantage of the DPS code family can

be summarized as follows: (1) good property in cross-correlation control; (2) short code length; (3) and easy to implement using fiber Bragg gratings (FBGs). The properties of this code based on numerical and simulation results have been proved and discussed. It has been shown that, the performance can be improved significantly when DPS code is used instead of DCS and RD codes. In order to backup our result, optical simulation software is carried out and the result is compared with calculated results. The calculation result was verified simulation by result where the two curves were almost identical. In addition, the bit rate and transmission distance have negative impacts on system performance in terms of BER due to dispersion effect. Additionally, the BER can be significantly improved when the DPS optimal channel spacing width is carefully selected where cross talk could be mitigated. In terms of channel spacing, best performance occurs at a spacing bandwidth between 0.8 (100 GHz) and 1.2 nm.

REFERENCES

1. J. A Salehi and C. A Brackett, "Code division multiple access techniques in optical fiber network – Part II: System performance analysis," *IEEE Transactions on Communications*, Vol. 37, 1989, pp. 834-842.
2. A. Stok and E. H. Sargent, "Lighting the local network: Optical code division multiple access and quality of service provisioning," *IEEE Network*, Vol. 14, 2000, pp. 42-46.
3. M. Kavehrad and D. Zaccarh, "Optical code-division-multiplexed systems based on spectral encoding of noncoherent sources," *Journal of Lightwave Technology*, Vol. 13, 1995, pp. 534-545.
4. E. D. J. Smith and R. J. Blaikie, and D. P Taylor, "Performance enhancement of spectral amplitude-coding optical CDMA using pulse-position modulation," *IEEE Transactions on Communications*, Vol. 46, 1998, pp. 1176-1185.
5. Z. Wei, H. M. H. Shalaby, and H. Ghafouri-Shiraz, "Modified quadratic congruence codes for fiber bragg-grating-based SAC-OCDMA," *Journal of Lightwave Technology*, Vol. 19, 2002, pp. 1209-1212.
6. Z. Wei and H. Ghafouri-Shiraz, "Code for spectral amplitude-coding optical CDMA systems," *Journal of Lightwave Technology*, Vol. 20, 2002, pp. 1284-1291.
7. T. H. Abd, S. A. Aljunid, H. A. Fadhil, R. B. Ahmad, and M. N. Junita, "Enhancement of performance of a hybrid SAC-OCDMA system using dynamic cyclic shift code," *Ukrainian Journal of Physical Optics*, Vol. 13, 2012, pp. 12-27.
8. S.-P. Tseng and J. S. We, "A new code family suitable for high-rate SAC OCDMA PONs applications," *IEEE Journal on Selected Areas in Communications*, Vol. 28, 2010, pp. 827-837.
9. H. A. Fadhil, S. A. Aljunid, and R. B. Ahmad, "Performance of random diagonal code for OCDMA systems using new spectral direct detection technique," *Optical Fiber Technology*, Vol. 15, 2009, pp. 283-289.
10. T. H. Abd, S. A. Aljunid, H. A. Fadhil, R. A. Ahmad, and N. M. Saad, "Development of a new code family based on SAC-OCDMA system with large cardinality for OCDMA network," *Optical Fiber Technology*, Vol. 17, 2011, pp. 273-280.

11. H. Y. Ahmed and K. S. Nisar, "Diagonal Eigenvalue Unity (DEU) code for spectral amplitude coding-optical code division multiple access," *Optical Fiber Technology*, Vol. 19, 2013, pp. 335-347.
12. H. Y. Ahmed, M. Almaleeh, H. A. Fadhil, S. A. Aljunid, A. Elyass, and N. M. Saad, "Performance analysis of spectral-amplitude-coding optical CDMA systems with new subtract exclusive OR detection (SED) using vectors combinatorial (VC) code," *International Journal for Light and Optics*, Vol. 123, 2012, pp. 1352-1359.

Hassan Yousif Ahmed received the B.Eng. in Computer Engineering (Network) and M.Sc in Computer Science and Information from Gezira University, Sudan in 2002 and 2007 and Ph.D. degree in Electrical and Electronic Engineering, University Tecknolgi PETRONAS, Malaysia. Currently he is an Associate Professor in Electrical Engineering Department, College of Engineering, Prince Sattam Bin AbdulAziz University. He is also the Dean Assistant for Quality and Development. His research interests are on computer network, wireless communications networks, and optical communications.

Zakaria M. Gharsseldien received his B.Sc. degree, M.Sc. degrees, and Ph.D. degree in Applied Mathematics from Al-Azhar University, Cairo, Egypt, in 1992, 1998, and 2003, respectively. He worked as a Lecturer in Department of Mathematics, Faculty of Science, Cairo, Al-Azhar University from 2003 to 2007. He is currently an Assistant Professor with the Department of Mathematics, Faculty of Arts and Science, Prince Sattam Bin AbdulAziz University from 2007. His current research interests are mathematical modeling in biology, medicine, and wireless communications, biomathematics, and bio fluid mechanics.

Syed Alwee Aljunid was born in Kedah, Malaysia. He obtained his Bachelor of Engineering in Computer and Communication Systems (First Class Honors) in 2001 and his Ph.D. degrees in Communication and Network Engineering from Universiti Putra Malaysia in 2005. Currently he is a Professor in the School of Computer and Communications, Universiti Malaysia Perlis (UniMAP). He is also the Dean of the Research Management and Innovation Centre (RMIC), Universiti Malaysia Perlis (UniMAP). His current research interests include Optical Fiber Communication, OCDMA technologies, Free Space Optic (FSO), OCDMA detection techniques and optical sensors.